Fundamental Investigation of Hingeless Rotor Aeroelastic Stability, Test Data and Correlation

Thomas H. Maier and David L. Sharpe
U.S. Army Aeroflightdynamics Directorate (ATCOM)

and

Joon W. Lim
Sterling Software

Ames Research Center
Moffett Field, California

ABSTRACT

An isolated, hingeless rotor with a fiber-reinforced composite root flexure was tested in hover and forward flight at realistic tip speeds. The purpose of the test was to measure the isolated rotor aeroelastic stability of bending/torsion coupled rotor blades over a range of flight conditions. The soft inplane rotor system was designed with low torsional stiffness to emphasize the effects of torsion. Damping in hover with collective pitch variations and in forward flight with airspeed, shaft angle and collective pitch variations are shown. The data quality is shown to be very good. Limited correlation with comprehensive analyses is shown. Agreement in hover is excellent while forward flight correlation is poor.

INTRODUCTION

The development of accurate analytical methods for aeroelastic stability predictions require careful comparison of calculations with experimental measurements. These methods, particularly at an early stage in their development, benefit from test data obtained with simplified rotor models whose properties are accurately characterized. The U.S. Army Aeroflightdynamics Directorate, AFDD, has conducted a number of experimental investigations of this type to study aeroelastic phenomena of cantilever rotor blades. One important simplification which allows researchers to concentrate on the structural dynamics and aerodynamics of the rotor system has been to isolate the rotor from hub motion. Early work with isolated rotors further restricted their efforts to Froude scale tip speeds in hover. A logical progression of structural models have been tested under these conditions. Initial work with rigid blades, tailored flap and lead-lag flexures and high torsional stiffness was reported in references 1-3. This work was further expanded in references 4-6 to investigate several design parameters on hingeless rotors. In addition, reference 4, emphasized the influence of torsion on the aeroelastic stability problem by designing a model with low first torsion frequency. Design parameters for bearingless hubs were tested in references 7 and 8. These experiments added the complexity of the bearingless hub while retaining simple airfoil and planform design for the blade. References 6 and 8, while not primarily isolated rotor tests, are included here because a portion of each test was for an isolated rotor.

Aeroelastic stability investigations of isolated rotors at AFDD were first extended to forward flight in an experimental test by McNulty.[9] This hingeless rotor had discrete flap and lead-lag flexures, a rigid blade and high torsional stiffness. Correlation efforts with data from this experiment have suffered from the low tip speeds and the unusual flight conditions due to the lack of a swashplate for trim control. These complicating factors coupled with the increasing need for data from torsionally soft rotor blades in forward flight, brought on by analytical advances in nonlinear structural dynamics and unsteady aerodynamics methods, have led to the present investigation.

Presented at the American Helicopter Society 51st Annual Forum, Fort Worth, TX, May 9-11, 1995.

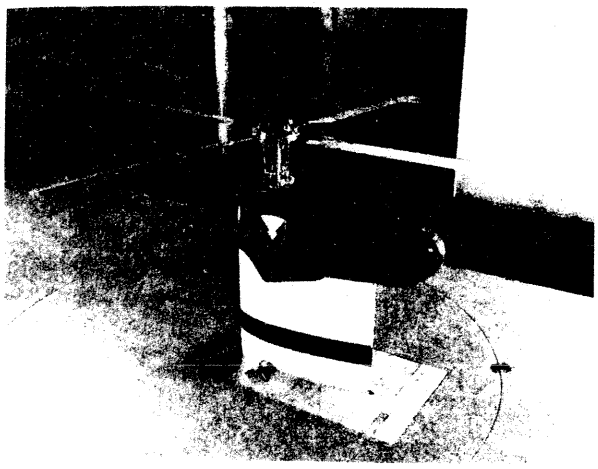

Fig. 1 Model rotor installed in the AFDD 7- x 10-Foot Wind Tunnel.

A 7.5 foot diameter, Mach-scale hingeless rotor has been designed, fabricated and tested at the AFDD. The primary purpose of this test was to obtain high quality forward flight data. Mach-scaling was used to provide aerodynamic section properties more representative of full-scale aircraft. Particular attention was paid to the pitch bearing design to avoid contamination of the aeroelastic stability with structural and kinematic nonlinearites. The model rotor was designed to test the capability of current and future analytic predictive tools. For this reason the structural and aerodynamic design was chosen to minimize the unknowns and/or approximations required by the analyst.

This paper presents a short description of the rotor, discusses the structural testing of the blade, and describes the hover and forward flight testing. Data from the tests are presented and compared with calculations from two comprehensive rotor codes, Comprehensive Analytical Model of Rotorcraft Aerodynamics and Dynamics, Johnson Aeronautics Version[10] (CAMRAD/JA) and Second Generation Comprehensive Helicopter Analysis System[11] (2GCHAS).

MODEL DESCRIPTION

The rotor is a 7.5 foot diameter, 3.4 inch chord hingeless rotor with rectangular planform, 2° pre-cone, zero pre-twist and NACA 0012 airfoil section. The nominal rotor speed of 1700 RPM results in a Reynolds number of 1.2×10^6 and a Mach number of 0.60 at the blade tip in hover. The rotor system may be seen as installed in the AFDD 7- by 10-Foot Wind Tunnel in figure 1. A planform drawing of the blade attached to the hub is shown in figure 2. The blade is composed of three distinct regions, flexure section, transition section, and constant blade section. A root cuff was bonded to every blade to ensure that a solid connection could be maintained between the blade and hub. Rotor control is achieved through a conventional swashplate which controls pitch on the blade root cuff inboard of any flap or lag flexure motion, resulting in negligible root end kinematic coupling. Fundamental blade flap and lag motion is accommodated with a composite root flexure 0.42 feet in length. A short, relatively stiff region provides the transition from the flexure to the blade airfoil section. Outboard of the transition is the constant blade section. The blade has no droop or sweep, and the mass center, tensile axis, aerodynamic center and elastic axis are coincident, or nearly so to the control axis which is located at the quarter chord.

The natural frequencies of the rotor system are shown in figure 3. The symbols show rotating and non-rotating measurements, and the curves represent calculations using the CAMRAD/JA eigenvalue analysis simulating *in-vacuo* conditions. Non-rotating frequencies were measured with the root fitting rigidly clamped to a massive, rigid structure. The first lead/lag frequency of the blades were tuned to match one another to within 0.05 Hz. by embedding a small weight into the tip of three of the blades. This was done to improve data quality by reducing blade-to-blade differences. Rotating frequencies were measured for the first lag mode only. The fundamental flap, lag and torsion frequencies calculated with CAMRAD/JA at the operating speed of 1700 RPM were 1.13, 0.71 and 2.56 per/rev, respectively.

Measured test stand frequencies are shown in figure 4 with the calculated fixed system rotor frequencies. The regressing lag mode frequency separation from the lowest stand frequency was 7.1 Hz. This separation was less than that suggested in reference 5 for a two-bladed rotor, but it was felt that these frequencies could not be raised without major redesign of the stand. The agreement between rotating frequency measurements and CAMRAD/JA calculations, shown in figure 3, indicate that the stand influence is slight for this four-bladed rotor.

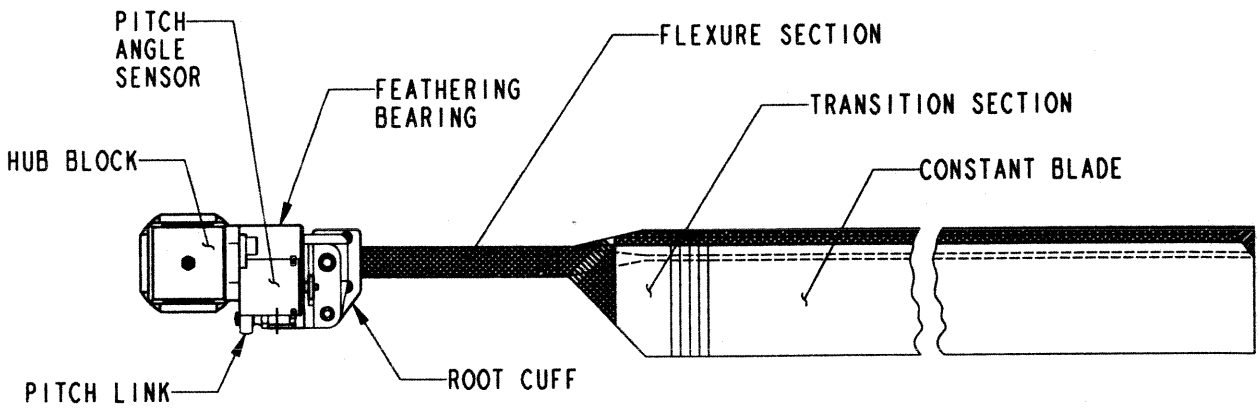

Fig. 2 Model rotor hub and blade.

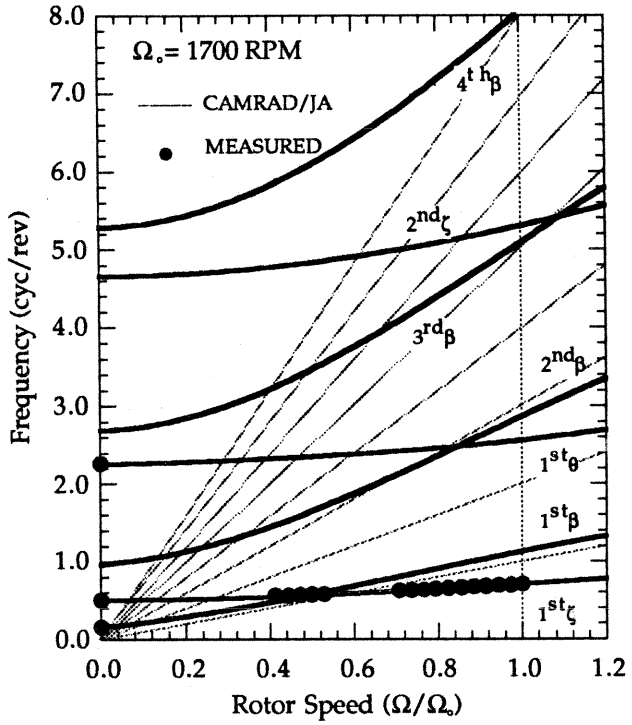

Fig. 3 Rotating blade frequencies diagram.

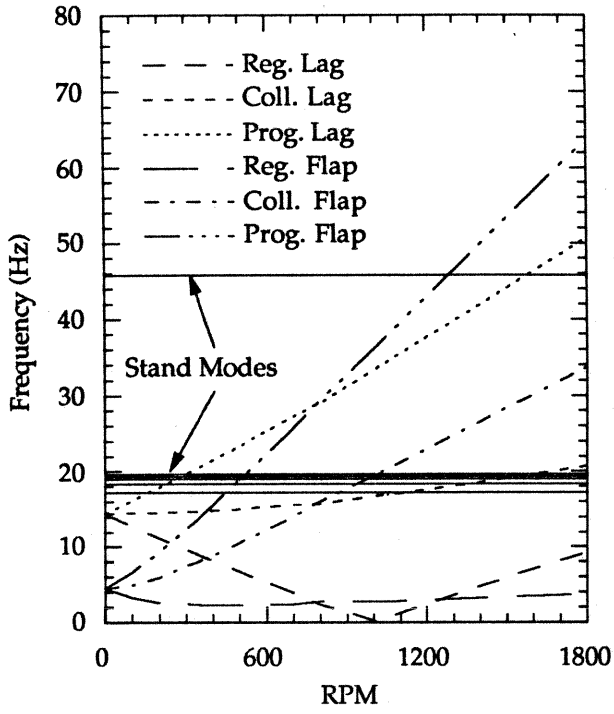

Fig. 4 Fixed system test stand and rotor fundamental flap and lead-lag frequencies.

Dynamic stability testing requires some means of exciting the mode or modes of interest. This was achieved during the test by using capability inherent in the test stand. The test stand, originally built by Sikorsky Aircraft for NASA, and designated the Rotor Test Rig (RTR), had been designed to include higher harmonic swashplate control. To accomplish this, low authority, high speed hydraulic actuators

were placed in series with each of the three high authority rotor trim control electric actuators. For this test, only one of the three hydraulic actuator was used to provide cyclic excitation at the regressing lag mode frequency.

BLADE PROPERTIES

One of the requirements of a rigorous research investigation is complete and accurate determination of model properties. The tests used to determine these properties are described below for three regions: root flexure, transition and blade. Within the root flexure and the blade all of the structural properties are assumed constant since the cross section design is constant. In the transition section the structural properties change continuously over the segment and it was not possible to measure the distribution. The resulting spanwise distribution of properties for the entire blade are tabulated in Appendix A.

The root flexure stiffness properties were measured on all of the completed blades while mass properties come from a single specimen. An accurate measure of the root flexure mass required the destruction of one blade. The 5 inch long root flexure section was cut off and weigh to determine mass. The polar moment of inertia was calculated using the weight and physical dimensions. Stiffness measurements were made on the completed blades with the root lug, transition section and constant blade intact. Flap and lag bending stiffness was measured using a three point bending set-up. There was some concern that the test would not be accurate with the rest of the blade attached so these measurements were compared with three measurements on a 5 inch long flexure only specimen. Three point bending, cantilever bending and free-free sonic tests on the 5 inch long flexure agreed well with flexure and integral blade test. Torsional stiffness was measured on all flexures as well by applying a torque to a short cantilevered segment and measuring the rotation.

The constant blade section of every blade used in dynamic testing was measured to determine structural properties. A short tip section was cut off to measure the running mass and center of gravity. This segment was also used to measure the polar moment of inertia by swinging the section from the trailing edge and measuring the pendulum frequency. Three point bending tests were made to provide flap and lag bending stiffness. Torsional stiffness was measured by applying a torque to the blade tip with the blade clamped just outboard of the transition section. As a further check on stiffness and inertial properties the flap, lag and torsion natural frequencies of the constant blade section were measured. The tensile axis was determined on a single specimen. For this test the blade section was placed in a pull test machine and the chordwise placement of the tensile load was adjusted until zero chordwise bending moment resulted. This also gave a measure of axial stiffness.

A transition section specimen was removed from a single blade to measure mass properties. The total weight and the spanwise and chordwise center of gravity were measured. This segment was also used to measure the polar moment of inertia by swinging the section from the trailing edge and measuring the pendulum frequency. No stiffness measurements were made for the short relatively stiff section. Reasonable assumptions were made to model the stiffness in this section for analytical correlation work. The values used may be seen in appendix A.

INSTRUMENTATION

The model instrumentation consisted mainly of rotating strain gauges. Each blade was instrumented with flap, lag, and torsion strain gauge bridges at two spanwise locations, 12% and 34% radius. The strain gauges at the inboard location were the main data signals which are reported here. The outboard gauges were used to monitor structural load during the test, and only one set of these was connected through the slip ring. Additionally, one blade was instrumented with two individual strain gauges to measure the local strain at the most critical location on the constant blade section just outboard of the transition section near the trailing edge of the airfoil. Blade pitch angle was measured at the root fitting on blades #1 and #3, using a rotational potentiometer and a Hall-effect transducer, respectively. Fixed system lateral and longitudinal acceleration just below the rotor hub were measured for safety and for rotor mass balancing. Shaft attitude was also measured. Local pressure and temperature were written down during the hover test. During the wind tunnel test, static and dynamic pressure as well as temperature were recorded with the other data. Rotor speed and azimuthal phase relations were obtained using a once per revolution optical encoder. The encoder was positioned to produce a spike when blade #1 was over

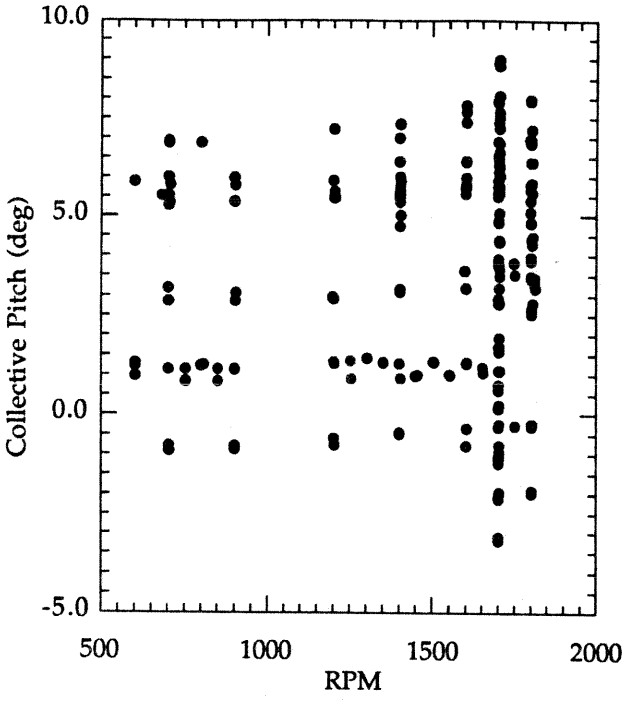

Fig. 5 Hover Test envelope.

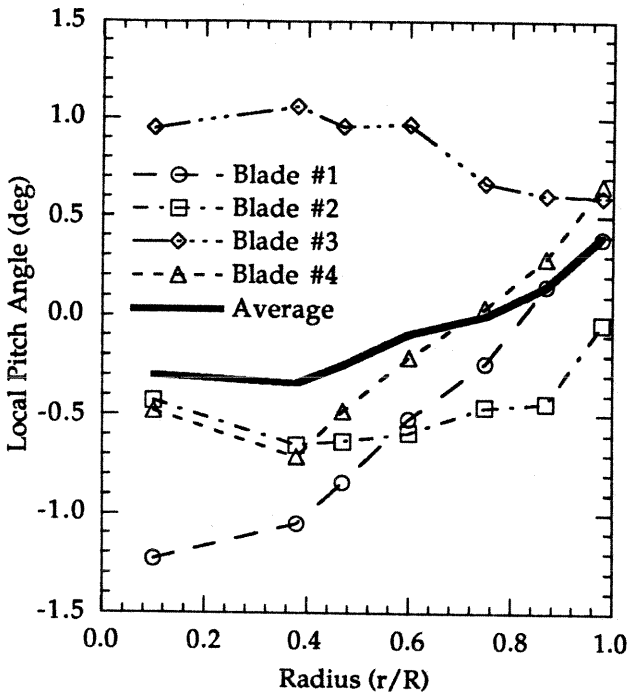

Fig. 6 Blade local pitch angle during hover testing.

the tail of the model, and the blade sequence going clockwise looking from above was: #1, #2, #3, #4.

The RTR test stand originally had a fixed system rotor balance. Unfortunately, with the balance flexibility included the lowest stand natural frequencies were very close to the rotor regressing lag frequency. Therefore, to improve the isolation of the rotor from the stand dynamics, it was necessary to lock out the balance. Structure was added to the test stand to bridge the balance, raising the stand frequencies above the regressing lag frequency as was shown in figure 4.

DATA ACQUISITION AND ANALYSIS

Simultaneous data were acquired for all rotor sensors over a period of 2 seconds at a sample rate of 1024 samples/sec. The voltage measurements were digitized and the strain gauge measurements were converted to bending moments based upon previous physical calibrations. The four individual blade root bending moments were transformed into the fixed system using the method of multiblade coordinates.[10] Individual rotating blade and non-rotating multiblade coordinate time history data were later analyzed for modal damping and frequency using the moving-block analysis technique.[11,12]

HOVER TEST DESCRIPTION

Hover testing was performed in the AFDD Anechoic Hover Test Chamber. This test chamber has a rectangular planform 26 feet by 32 feet and is 28 feet in height. Inflow for the rotor is drawn into the chamber through ten 2 foot by 6 foot ducts located along the ceiling. Recirculation can be reduced by passing the rotor wake through an annular diffuser located on a moveable platform, and exhausting the flow out of the chamber along the floor on opposite sides of the room. Figure 5 depicts the hover test envelope, in terms of collective pitch and rotor speed, that was obtained with the 2° precone hub.

When acquiring data in hover the shaft angle was set to zero degrees. The rotor was set to the desired rotor speed and collective pitch angle. Low amplitude cyclic pitch excitation was applied and the frequency was adjusted until the lead/lag response of blade #1 reached a maximum. The amplitude of excitation was then adjusted to give lead/lag response just below the structural limit. The excitation was stopped and 2 seconds of data were acquired.

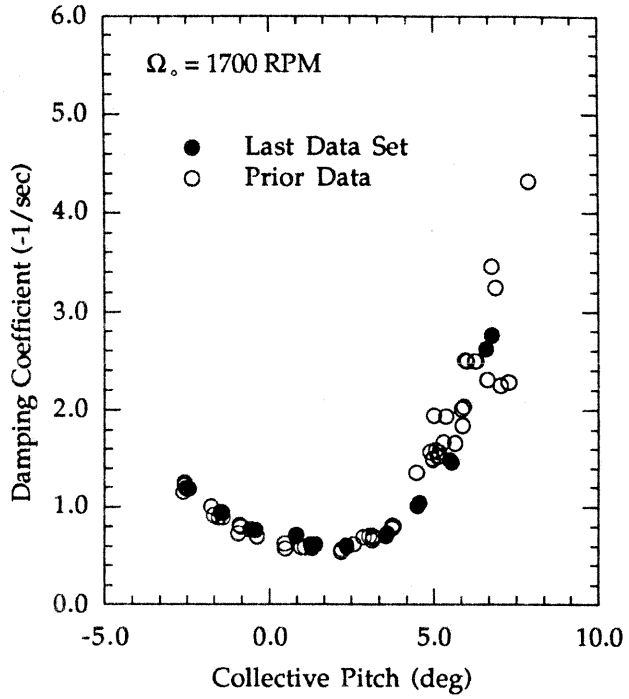

Fig. 7 Hover test regressing lag mode damping; last data acquired, and all data prior to final blade tracking adjustment; 1700 RPM.

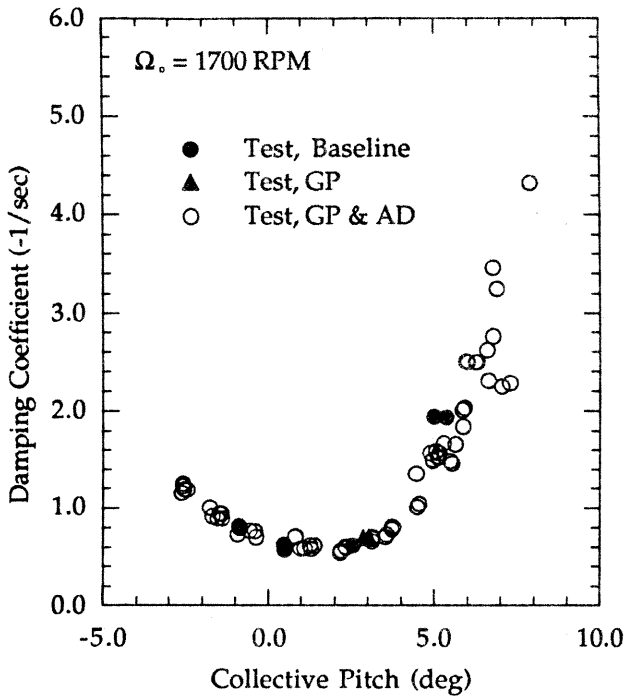

Fig. 8 Hover test regressing lag mode damping; baseline data, data acquired with ground plane and data acquired with ground plane and annular diffuser; 1700 RPM.

During blade tracking it was discovered that the blades had twist irregularities. Although the blade mold was machined with zero twist, each blade had unique twist discrepancies. An inclinometer was used to measure the local pitch angle along the blade at 6 radial locations with respect to the root cuff. Figure 6 shows the radial distribution of the local pitch angle for the hover test blade set prior to removing the rotor from the hover test chamber. It contains the pitch due to the pitch link adjustments as well as the radial deviation from nominal zero twist. Also shown in the figure is the average pitch distribution of all blades. Collective pitch angles are defined relative to the pitch distribution shown here with the average of all blades at 75% radius equal to zero. Because the root pitch angle of all the blades were measured at the end of the test, the exact pitch angle relationship shown here is only valid for the data taken prior to the last blade tracking adjustment. Figure 7 compares the last set of data where the root pitch angles were measured with all data taken prior to the last tracking adjustment. The agreement between data is excellent, indicating that the tracking adjustments were small.

The maximum collective pitch setting for which data were acquired was limited by structural loads in the flexure. Ideally, there are no oscillatory loads in the hover condition. The test set-up, however, was not ideal. The balance hardware and hydraulic plumbing on the RTR test stand is below the rotor at 0° azimuth. In this location the flow of the rotor is blocked over a portion of the disk. Also, the rectangular cross section of the hover chamber is thought to create 4P loads due to asymmetries in the recirculation. To reduce oscillatory loads and hence increase the collective pitch range of the test, several configuration changes were attempted. The most successful configuration incorporated a 56 inch diameter ground plan 10 inches below the rotor. In addition, the test chamber moveable platform, with an 8 foot diameter annular diffuser, was placed 8 inches below the non-rotating tip path plane just above the rotor balance hardware. Data acquired in this configuration (GP & AD), with the ground plane only (GP) and in the baseline configuration are compared in figure 8. In all configurations the doors on either side of the room were open to exhausted the flow. Over the range of collective pitch angles where

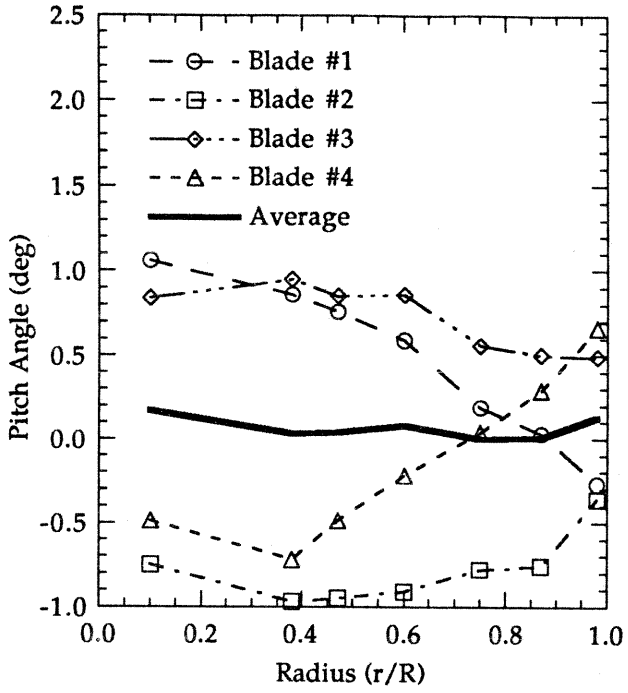

Fig. 9 Blade local pitch angle during forward flight testing.

measurements are available these data show no significant influence on lead/lag damping due to the test section configuration. An increase in collective pitch for which data could be obtained was increased by 2.5° by using the ground plane and annular diffuser.

FORWARD FLIGHT TEST DESCRIPTION

Forward flight testing took place in the AFDD 7- by 10-Foot Wind Tunnel. When acquiring data in forward flight the shaft angle was set, the rotor speed brought up to 1700 RPM, collective pitch was set and the tunnel airspeed was slowly increased to the desired value while the rotor cyclic pitch was adjusted to maintain low oscillatory flapping loads. Once on the air speed, the collective was re-adjusted to get as close as possible to the desired value and the cyclic pitch adjusted to minimize the 1P flapping moment at 12% radius. Low amplitude cyclic excitation was applied and the frequency was adjusted until the lead/lag response of blade #1 reached a maximum. The amplitude of excitation was then adjusted to give lead/lag response just below the structural limit. The excitation was shut off and 2 seconds of data were acquired. The forward flight test envelope for which data were collected with the 2° precone hub is depicted in table 1. In the table the advance ratio range for different shaft angles, α_s (positive nose-up), and collective pitch angles, θ_o, is shown. The corresponding trim variables (Advance Ratio, μ; Collective Pitch, θ_0,; Lateral Cyclic Pitch, θ_c,; Longitudinal Cyclic Pitch, θ_s; Root Flap Moment at 12% Radius, $M\beta_{@12\%R}$) for the damping measurements which are shown in this paper are included in Appendix B.

Table 1. Forward Flight Envelope

	$\theta_o = 3°$	$\theta_o = 4°$	$\theta_o = 5°$	$\theta_o = 6°$
$\alpha_s = -6°$	.0 - .30	.0 - .30	.0 - .30	.05 - .35
$\alpha_s = -3°$	.0 - .30	.0 - .30	-	-
$\alpha_s = 0°$	.0 - .30	-	-	-

Prior to data acquisition the root pitch of the blades were adjusted to improve blade track. A small balsa wood triangular cross-section wedge was also attached to the trailing edge of blade #1 to improve the track. Track was checked in hover and up to advance ratio 0.30 at 3° collective pitch and found to be within one blade thickness. After the track was satisfactory the root pitch on the blades was not changed. The spanwise distribution of static pitch angle for the rotor system during forward flight testing is shown in figure 9. It contains the pitch due to the pitch link adjustments as well as the radial deviation from nominal zero twist. Collective pitch angles are defined relative to the pitch distribution shown here with the average of all blades at 75% radius equal to zero. Differences between figures 6 and 9 are due to tracking changes and a replacement blade in the blade #1 position.

The influence on lead/lag damping due to blade-to-blade differences may be seen by comparing the damping measured on each blade. Figure 10 shows the individual blade damping measurement with advance ratio as compared with the regressing lag mode damping from the multiblade cyclic coordinate for shaft angle -6° and collective pitch 3°. The multiblade cyclic coordinate damping is shown as a solid symbol. The individual blade damping form a band around the multiblade cyclic coordinate damping. Although it appears as data scatter, the individual blade damping values are repeated for most of the test points. Therefore, while not the intent of this test, these measurements might be useful for validation of dissimilar blade analyses. The remainder of this paper will present only the

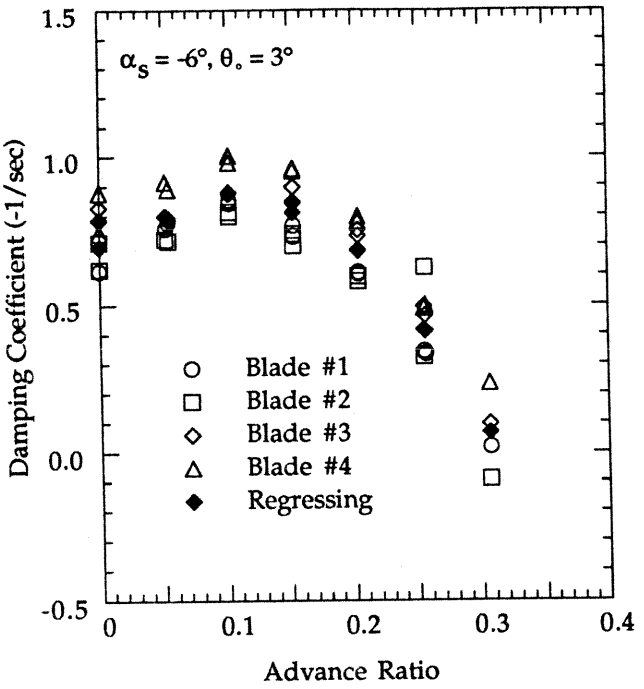

Fig. 10 Forward flight test individual blade damping and multiblade cyclic coordinate regressing lag mode damping with advance ratio; 1700 RPM.

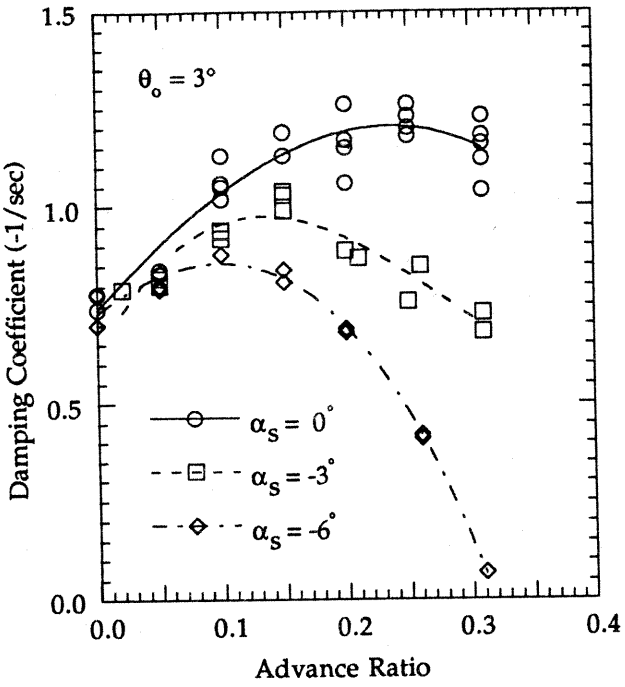

Fig. 11 Forward flight test regressing lag mode damping with advance ratio for three different shaft angles; 1700 RPM.

multiblade cyclic coordinate regressing mode damping coefficient.

The rotor damping was measured for three different shaft angles: α_s = 0°, -3°, and -6°. Figure 11 shows the damping coefficient with advance ratio at 3° collective pitch for these three shaft angles. Least squares fit polynomial curves have been drawn to help clarify the trend for each shaft angle. The damping is seen to increase with advance ratio at first and then to drop rapidly as the velocity of air flow normal to the rotor disk increases with tunnel speed and shaft angle. This trend suggests a dependency on rotor thrust. Unfortunately, with the rotor balance locked out thrust measurements were precluded. The root flap moment gauges were measured on all blades and the average of these is an indication of rotor thrust. Figure 12 shows damping plotted against the average root flap moment at 12% radius for the three airspeed sweeps of figure 11. A least squares fit line has been drawn to identify the trends. The relationship is quite strong as indicated by the grouping of the data. Therefore, it is important that analytical models match the flap moment of the root section to obtain good correlation with the data shown here.

The damping trend with increasing collective pitch was measured at -6° shaft angle. Figure 13 shows the damping coefficient with advance ratio for collective pitch angles equal to 3.0°, 3.9°, 4.9° and 5.9°. Again, a least squares fit polynomial has been drawn to help clarify the trends. It is seen in this figure that the data scatter increases somewhat as the damping level increases. Greater data scatter is also apparent near hover and at high advance ratio.

CAMRAD/JA MODEL

The CAMRAD/JA math model of the rotor has evolved with the design. The structural model, while based on measured structural properties, was adjusted to match frequency tests. In particular, a model of the constant blade section was developed and validated with the blade constant section frequency test. The polar moment of inertia of the constant blade section was increased slightly to agree with the torsion frequency measurement. This was combined with the

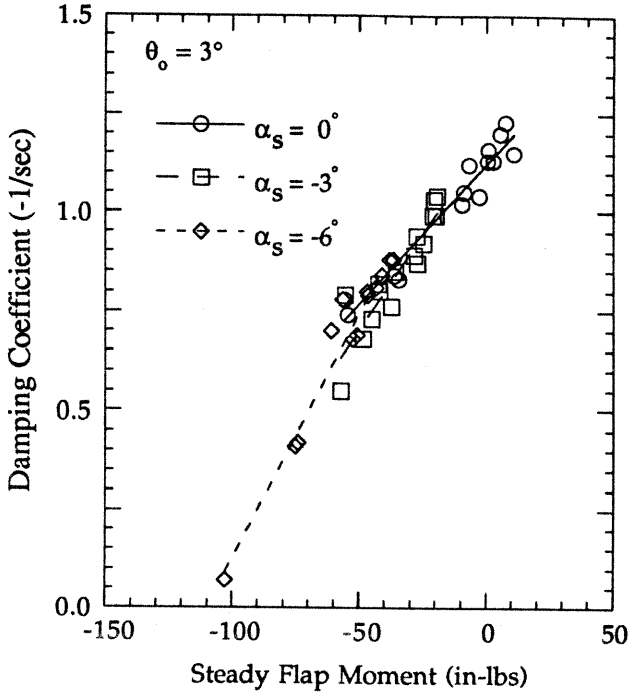

Fig. 12 Forward flight test regressing lag mode damping with steady flap moment at 12% radius for three different shaft angles; 1700 RPM.

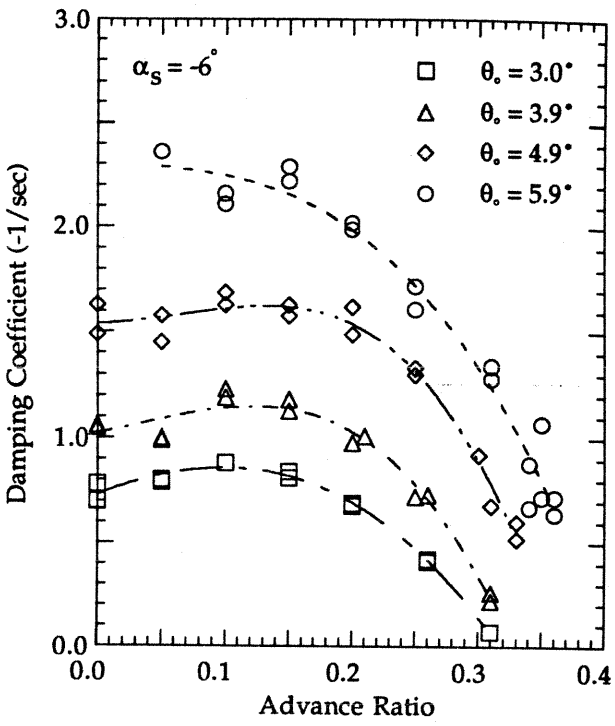

Fig. 13 Forward flight test regressing lag mode damping with advance ratio for four different collective pitch angles; 1700 RPM.

transition and root flexure properties to model the complete blade. When the calculated frequencies for the entire blade were slightly different than the nonrotating measured frequencies, the flexure stiffness was adjusted. The final spanwise distribution of properties used in the CAMRAD/JA calculation are tabulated in Appendix A. Six bending modes and three torsion modes were used with the cantilever root end boundary condition in the CAMRAD/JA trim calculation. The program allows the user to set the number of modes used to calculate the steady deflected shape about which the eigenanalysis is solved. This parameter, DOFT, was set to 4 for the baseline calculations. Structural damping of the bending and torsion modes was set at 1% to match nonrotating measurements.

The aerodynamic model in CAMRAD/JA is described in detail in reference 10. The blade was divided into 15 aerodynamic segments and a NACA 0012 C81 airfoil table provided lift, drag and moment with angle of attack and Mach number. The baseline calculation used uniform inflow with a hover inflow correction factor equal to 1.0, tip loss equal to 0.98 and no inflow degrees of freedom. Forward flight calculations were made with the free wake inflow model.

2GCHAS MODEL

The rotor was modeled in 2GCHAS using a single blade option. The blade was discretized into ten nonlinear beam elements: one beam element for the rigid hub extension, three beam elements for the flexure section, three elements for the transition section, and three elements for the blade section. Seven aerodynamic segments were used for the blade airfoil beginning at the blade root cutout and extending to the tip. The nonlinear aerodynamic model (table look-up) with linear unsteady aerodynamic effect, was used for the calculations, coupled with uniform inflow (empirical factor of 1.0) and, where specified, free wake analysis. The measured structural damping of 1% (ζ = 0.5%) was included for the analysis. For the free wake, the tip vortex core radius was set to 3.2% of the blade radius. The two degree precone was modeled such that the

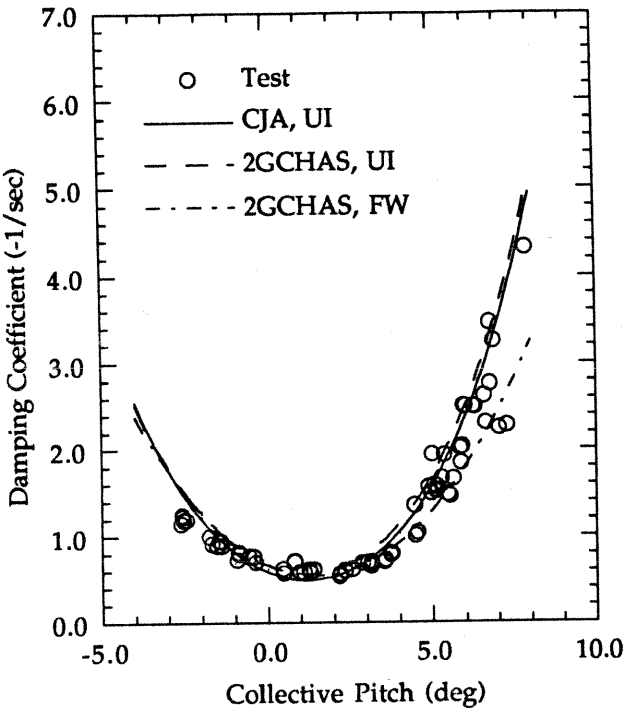

Fig. 14 Hover test regressing lag mode damping with CAMRAD/JA and 2GCHAS calculations; 1700 RPM.

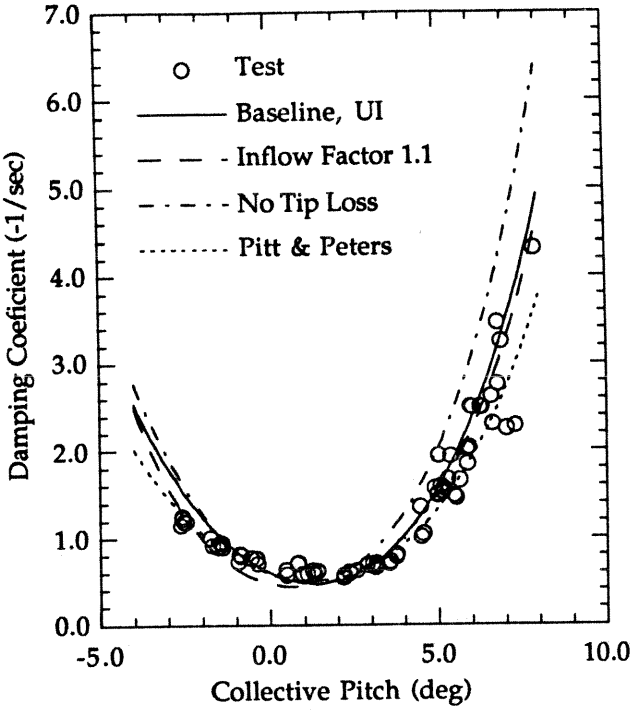

Fig. 15 Hover test regressing lag mode damping with CAMRAD/JA aerodynamic modeling variations; 1700 RPM.

beam elements and aerodynamic segments were aligned along the precone axis.

COMPARISON OF THEORY AND TEST DATA

Calculated results for hover using CAMRAD/JA and 2GCHAS are shown with test data in figure 14. The 2GCHAS calculation demonstrates the difference between uniform inflow and free wake for the trim solution about which the eigenanalysis is solved. The inclusion of the free wake reduces the calculated damping, especially at large positive collective pitch. Excellent agreement is seen between CAMRAD/JA and 2GCHAS using uniform inflow. The uniform inflow calculations also show excellent correlation with the data except for the negative collective pitch values.

Several aerodynamic parameters were adjusted within the CAMRAD/JA calculation to examine their influence on lead/lag damping. The 3 state Pitt and Peters dynamic inflow model was seen to improve the correlation for negative collective pitch angles. Increasing the hover inflow correction factor from 1.0 to 1.1 was seen to produce a slight drop in the calculated damping and removing the tip loss was seen to dramatically increase the damping. These results are compared with the baseline calculation and the test data in figure 15. The later two parameters directly affect rotor thrust and should be set to values which provide the best correlation with rotor performance. They are included here to emphasize the sensitivity of lead/lag damping to simple inflow modeling features.

The excellent correlation shown in figures 14 and 15 using CAMRAD/JA was not achieved until after the data were obtained. Pre-test calculations using showed poor correlation with the data. This was due to the parameter DOFT which determines the number of modes used to calculate the steady deflected shape about which the eigenanalysis is solved. The CAMRAD/JA baseline files initialize this parameter at 2. Therefore, the deflected shape was composed of the fundamental flap and lag modes only. Adjusting this parameter to include the second and third flap mode significantly improved the correlation. This is

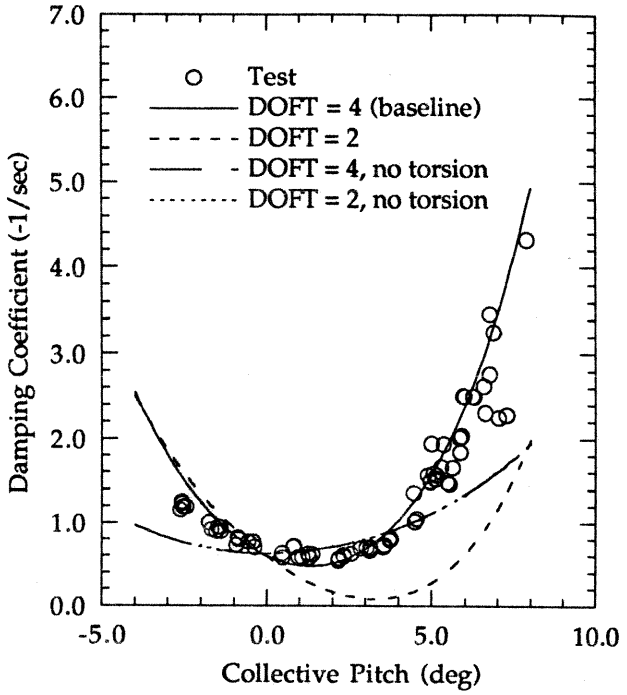

Fig. 16 Hover test regressing lag mode damping with CAMRAD/JA structural modeling variations; 1700 RPM.

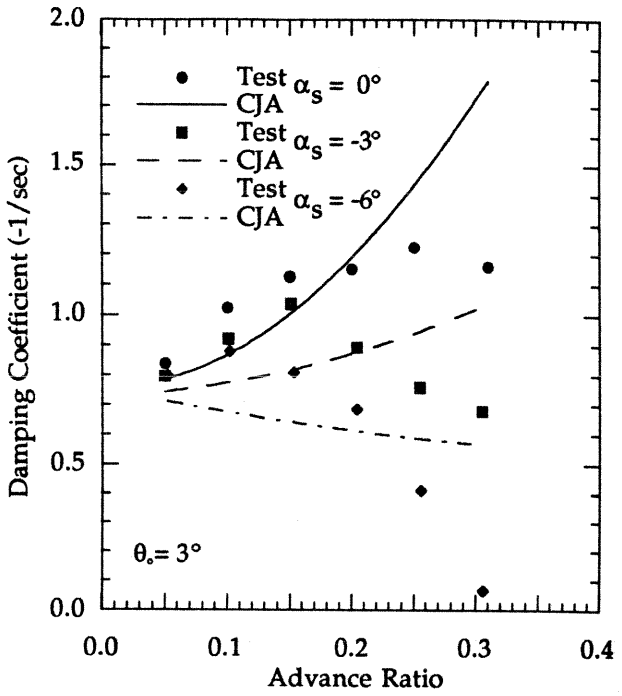

Fig. 17 Forward flight regressing lag mode damping with CAMRAD/JA free wake calculations for three different shaft angles; 1700 RPM.

shown in figure 16, with and without the influence of the torsion degrees of freedom. Pre-test calculations using 2GCHAS required no adjustment in the structural or aerodynamic modeling for the agreement shown here.

Having seen excellent correlation between analysis and test data in hover, the forward flight correlation is disappointing. Figure 17 shows CAMRAD/JA calculated damping with advance ratio for the three shaft angles measured. The free wake was used to calculate the periodic equilibrium solution and a constant coefficient approximation was made to simplify the stability analysis. CAMRAD/JA predicts the difference in damping between the different shaft angles, but it does not predict the destabilizing trend with advance ratio. It is also interesting that the data shows a convex trend with advance ratio, while the calculated trend is concave.

CONCLUDING REMARKS

An isolated rotor test on a 7.5 foot diameter small scale hingeless rotor has been conducted at representative tip speeds in hover and forward flight. Regressing lag mode damping was measured over a variety of flight conditions. Measured data was compared with calculations from comprehensive rotor codes. The major findings of the study are as follows:

1. Forward flight stability data were collected which show clear trends due to the influence of shaft angle and collective pitch.

2. Hover stability data were collected which show clear trends due to the influence of collective pitch.

3. The lead-lag damping of this model is highly sensitive to the root flap moment measured at 12% span.

4. Both CAMRAD/JA and 2GCHAS calculations show excellent correlation with the hover data.

5. Individual blade damping differences were measured which are presumed to be due to small discrepancies in blade twist. The twist discrepancies were measured and the damping differences are, for the most part, repeatable.

6. Initial attempts to correlate with this data in forward flight showed poor correlation between measurement and analysis.

ACKNOWLEDGMENTS

The authors extend their appreciation to the Rotorcraft Aeromechanics Branch at NASA Ames Research Center for the RTR test stand and accompanying advice; Sikorsky Aircraft for the use of their hydraulic servo valves; NASA Ames Research Center Engineering, Machine Shop, Model Shop and R&QA for their work on the model; and most of all the AFDD Experimental Support Team for their instrumentation magic, tirelessness during monotony and can do attitude!

REFERENCES

[1] Ormiston, R.A. and Bousman, W.G., "A Theoretical and Experimental Investigation of Flap-Lag Stability of Hingeless Helicopter Rotor Blades," NASA TM X-62-179, August 1972.

[2] Ormiston, R.A. and Bousman, W.G., "A Study of Stall Induced Flap-Lag Instability of Hingeless Rotors, "*Journal of the American Helicopter Society*, Vol. 29, No. 1, January 1975, pp. 20-30.

[3] Bousman, W.G., Sharpe, D.L., Ormiston, R.A., "An Experimental Study of Techniques for Increasing the Lead-Lag Damping of Soft Inplane Hingeless Rotors," Preprint No. 1035, Proceedings AHS 32nd National Forum, Washington, D.C., May 1976.

[4] Sharpe, David L., An Experimental Investigation of the Flap-Lag-Torsion Aeroelastic Stability of a Small-Scale Hingeless Helicopter Rotor in Hover," NASA TP 2546, AVSCOM TR 85-A-9, 1986.

[5] Bousman, W.G., "The Effects of Structural Flap-Lag and Pitch-Lag Coupling on Soft Inplane Hingeless Rotor Stability in Hover," NASA TP 3002, AVSCOM TR 89-A-002, 1990.

[6] Weller, W.H., "Relative Aeromechanical Stability Characteristics for Hingeless and Bearingless Rotors," *Journal of the American Helicopter Society*, Vol. 35, No. 3, July 1990, pp. 68-77.

[7] Dawson, S., "An Experimental Investigation of the Stability of a Bearingless Model Rotor in Hover," *Journal of the American Helicopter Society*, Vol. 28, No. 4, October 1983, pp. 29-34.

[8] Weller, W.H., and Peterson, R.L., "Inplane Stability Characteristics for an Advanced Bearingless Main Rotor Model," *Journal of the American Helicopter Society*, Vol. 29, No. 3, July 1984, pp. 45-53.

[9] McNulty, M.J., "Flap-Lag Stability Data for a Small-Scale Isolated Hingeless Rotor in Forward Flight," NASA TM 102189, USAAVSCOM TR 89-A-003, April 1989.

[10] Johnson Wayne, "CAMRAD/JA; A Comprehensive Analytical Model of Rotorcraft Aerodynamics and Dynamics; Johnson Aeronautics Version; Volume I, Theory Manual," Johnson Aeronautics, Palo Alto, California, 1988.

[11] Anon, "2GCHAS Theory Manual, Version 2.3," U.S. Army Aeroflightdynamics Directorate (ATCOM), March 1994.

[12] Hohenemser, Kurt H. and Yin, Sheng-Kuang, "Some Applications of the method of Multiblade Coordinates," *Journal of the American Helicopter Society*, Vol. 17, No. 3, July 1972, pp. 3-12.

[13] Hammond, Charles E. and Doggett, Robert V., Jr., "Determination of Subcritical Damping by Moving-Block/Randomdec Application," NASA Symposium on Flutter Testing Techniques, NASA SP-415, October 1975, pp. 59-76.

[14] Bousman W.G., and Winkler D.J., "Application of the Moving-Block Analysis," Proceedings, AIAA/ASME/ASCE/AHS 22nd Structures, Structural Dynamics, and Materials Conference, Atlanta, Georgia, April 1981, pp. 755-763.

APPENDIX A Structural Properties

Table A1. Measured Structural Properties.

Radius (r/R)	Mass/ft (slugs/ft)	Polar Inertia/ft (slug-ft)
0.104	0.00575	2.42E-06
0.216	0.00575	2.42E-06
0.216	0.00981	4.12E-05
0.306	0.00981	4.12E-05
0.306	0.00633	3.57E-05
1.000	0.00633	3.57E-05

Radius (r/R)	Flap Stiffness (lbs-ft^2)	Chord Stiffness (lbs-ft^2)	Torsion Stiffness lbs-ft^2/rad	Axial Stiffness (lb)
0.104	52.076	268.58	22.188	1.022E+06
0.216	52.076	268.58	22.188	1.022E+06
0.216	-	-	-	-
0.306	-	-	-	-
0.306	53.728	1698.90	26.395	4.796E+05
1.000	53.728	1698.90	26.395	4.796E+05

Radius (r/R)	Elastic Axis aft of Feathering Axis (x/R)	Center of Garvity aft of Feathering Axis (x/R)
0.104	0.00000	0.00000
0.216	0.00000	0.00000
0.216	0.00000	0.00476
0.306	0.00000	0.00476
0.306	0.00000	0.00045
1.000	0.00000	0.00045

Table A2. Structural Properties Used in CAMRAD/JA Calculation.

Radius (r/R)	Mass/ft (slugs/ft)	Polar Inertia/ft (slug-ft)
0.104	0.00575	2.42E-06
0.216	0.00575	2.42E-06
0.216	0.00981	4.12E-05
0.306	0.00981	4.12E-05
0.306	0.00633	3.76E-05
1.000	0.00633	3.76E-05

Radius (r/R)	Flap Stiffness (lbs-ft^2)	Chord Stiffness (lbs-ft^2)	Torsion Stiffness lbs-ft^2/rad	Axial Stiffness (lb)
0.104	45.523	268.58	22.188	1.022E+06
0.216	45.523	268.58	22.188	1.022E+06
0.216	56.904	537.16	44.376	*
0.306	67.160	3397.79	52.791	*
0.306	53.728	1698.90	26.395	4.796E+05
1.000	53.728	1698.90	26.395	4.796E+05

Radius (r/R)	Elastic Axis aft of Feathering Axis (x/R)	Center of Garvity aft of Feathering Axis (x/R)
0.104	0.00000	0.00000
0.216	0.00000	0.00000
0.216	0.00000	0.00476
0.306	0.00000	0.00476
0.306	0.00000	0.00045
1.000	0.00000	0.00045

*Not CAMRAD/JA Input.

APPENDIX B Trim Measurements

Table B1. Trim conditions α_s = 0°, θ = 3.0°

μ (-)	θ_0 (deg)	θ_c (deg)	θ_s (deg)	Mβ @12%R (in-lbs)
0.00	3.04	-0.01	0.00	-55.8
0.00	3.09	-0.01	0.00	-54.6
0.05	3.09	1.11	0.93	-34.3
0.05	3.07	1.09	0.98	-36.3
0.10	3.08	0.27	1.37	-8.9
0.10	3.04	0.25	1.38	-9.7
0.15	2.99	-0.10	1.75	0.5
0.15	2.94	-0.04	1.77	2.9
0.20	3.06	-0.62	2.13	10.8
0.25	2.96	-0.85	2.37	7.7
0.25	2.94	-0.83	2.39	5.5
0.31	2.96	-1.23	2.75	-2.9
0.31	2.97	-1.28	2.77	0.7
0.31	2.94	-1.22	2.79	-6.9

Table B2. Trim conditions α_s = -3°, θ = 3.0°

μ (-)	θ_0 (deg)	θ_c (deg)	θ_s (deg)	Mβ @12%R (in-lbs)
0.01	2.98	-0.06	0.03	-57.3
0.02	3.06	-0.01	0.01	-55.4
0.05	2.91	0.73	1.10	-42.3
0.05	2.96	0.74	1.12	-41.8
0.10	2.83	0.13	0.86	-27.3
0.10	2.92	0.26	1.09	-24.5
0.15	2.95	-0.26	1.27	-19.3
0.15	2.92	-0.25	1.28	-20.5
0.20	2.93	-0.83	1.70	-28.3
0.21	2.96	-0.84	1.69	-27.2
0.25	2.93	-0.81	1.53	-37.3
0.26	2.92	-0.80	1.56	-35.3
0.31	2.98	-1.05	1.63	-45.0
0.31	2.95	-1.09	1.61	-48.3

Table B3. Trim conditions α_s = -6°, θ = 3.0°

μ (-)	θ_0 (deg)	θ_c (deg)	θ_s (deg)	Mβ @12%R (in-lbs)
0.00	3.15	-0.04	0.11	-56.4
0.00	2.82	0.00	0.00	-61.1
0.05	2.91	0.41	1.12	-46.5
0.05	2.86	0.45	1.14	-46.9
0.10	2.98	0.10	0.95	-36.4
0.10	2.90	0.19	0.94	-38.0
0.15	2.96	-0.45	1.14	-40.9
0.15	2.95	-0.49	1.12	-43.3
0.20	3.06	-0.59	0.98	-52.5
0.20	3.05	-0.59	0.98	-51.0
0.26	2.93	-0.69	1.05	-74.1
0.26	2.92	-0.73	1.12	-75.1
0.31	2.88	-1.05	1.37	-102.9

Table B4. Trim conditions α_s = -6°, θ = 3.9°

μ (-)	θ_0 (deg)	θ_c (deg)	θ_s (deg)	Mβ @12%R (in-lbs)
0.00	3.97	0.35	0.37	-45.3
0.00	3.97	0.36	0.42	-44.7
0.05	3.90	0.59	1.23	-33.5
0.05	3.92	0.44	1.28	-32.5
0.10	3.88	0.02	1.40	-17.6
0.10	3.99	0.10	1.25	-15.6
0.15	3.94	-0.48	1.39	-17.5
0.15	3.94	-0.52	1.41	-16.1
0.21	3.99	-0.94	1.70	-30.9
0.20	3.90	-0.88	1.71	-36.0
0.26	3.91	-0.94	1.63	-50.7
0.25	4.00	-0.97	1.57	-45.8
0.31	3.90	-1.29	1.43	-68.7
0.31	3.90	-1.30	1.45	-71.6

Table B5. Trim conditions $\alpha_s = -6°$, $\theta = 4.9°$

μ (-)	θ_0 (deg)	θ_c (deg)	θ_s (deg)	$M\beta_{@12\%R}$ (in-lbs)
0.00	4.95	0.26	0.46	-27.1
0.00	5.03	0.20	0.38	-26.8
0.05	4.91	0.53	1.38	-15.1
0.05	4.85	0.59	1.41	-16.4
0.10	4.91	-0.17	1.83	8.9
0.10	5.05	-0.22	1.85	11.7
0.15	4.96	-0.87	2.05	13.8
0.15	4.96	-0.91	2.06	14.9
0.20	4.96	-1.36	2.16	4.4
0.20	4.95	-1.39	2.14	3.4
0.25	4.95	-1.37	2.19	-14.3
0.25	4.97	-1.40	2.19	-14.3
0.30	4.95	-1.65	2.31	-38.8
0.31	4.92	-1.67	2.32	-38.8
0.33	4.91	-1.75	2.17	-48.3
0.33	4.88	-1.69	2.17	-53.2

Table B6. Trim conditions $\alpha_s = -6°$, $\theta = 5.9°$

μ (-)	θ_0 (deg)	θ_c (deg)	θ_s (deg)	$M\beta_{@12\%R}$ (in-lbs)
0.05	5.80	0.31	1.68	1.5
0.10	5.72	-0.23	2.22	29.3
0.10	5.73	-0.26	2.24	26.8
0.15	5.95	-1.48	2.66	41.9
0.15	5.94	-1.25	2.42	41.7
0.20	5.94	-1.93	2.91	32.1
0.20	5.94	-1.98	2.92	31.0
0.25	5.88	-2.34	2.94	12.1
0.25	5.95	-2.27	3.04	15.2
0.31	5.97	-2.28	3.24	-8.0
0.31	6.00	-2.35	3.99	-9.0
0.34	5.88	-2.34	3.31	-31.7
0.34	5.90	-2.36	3.29	-30.8
0.35	5.92	-2.29	3.46	-34.5
0.35	5.91	-2.27	3.48	-34.8
0.36	5.84	-2.20	3.04	-34.8
0.36	5.83	-2.23	2.98	-40.8